1959

Range-energy measurements for 742-Mev protons.

Ward, John E.

RANGE-ENERGY MEASUREMENTS FOR 742-MEV PROTONS

JOHN E. WARD

UCRL-8762
Physics and
Mathematics

UNIVERSITY OF CALIFORNIA
Lawrence Radiation Laboratory
Berkeley, California

Contract No. W-7405-eng-48

RANGE-ENERGY MEASUREMENTS FOR 742-Mev PROTONS

John E. Ward

May 4, 1959

Submitted in partial fulfillment
of the requirements for the degree of

MASTER OF SCIENCE

in

PHYSICS

United States Naval Postgraduate School
Monterey, California

Printed for the U. S. Atomic Energy Commission

Printed in USA. Price $1.25. Available from the
Office of Technical Services
U. S. Department of Commerce
Washington 25, D. C.

RANGE-ENERGY MEASUREMENTS FOR 742-Mev PROTONS

John E. Ward

Lawrence Radiation Laboratory
University of California
Berkeley, California

May 4, 1959

ABSTRACT

This is a proposal for an experiment to measure the relative stopping powers of Be, Al, Fe, Cu, Ag, W, Pb, and U by magnetically analyzing the degraded proton energies of the 742-Mev proton beam of the Berkeley cyclotron after passage through the absorbing elements.

RANGE-ENERGY MEASUREMENTS FOR 742-Mev PROTONS

John E. Ward

Lawrence Radiation Laboratory
University of California
Berkeley, California

May 4, 1959

I. INTRODUCTION

If a charged particle passes through a substance with sufficient energy that the valence-shell effects--i.e., atomic binding--can be neglected, the average rate of energy loss due to ionization only is expressed by the well-known Bethe equation,[1]

$$-\frac{dE}{dx} = \frac{4\pi e^4 z^2}{mv^2} NZ \left[\ln \frac{2mv^2}{I} - \ln(1-\beta^2) - \beta^2 \right], \qquad (1)$$

where e and m refer to the electronic charge and mass, ez is the charge of the incident particle, NZ is the number of electrons per unit volume of the stopping element, and I is the "mean excitation potential" of the atoms in the stopping element.

The development of this formula makes use of the Born approximation, which requires the orbital velocity of the electrons to be small compared with the velocity of the incident particle. A proton with a kinetic energy greater than 2 Mev satisfies this condition.[2]

It can be seen that the stopping power depends only on the velocity and charge of the incident particle and not its mass, and the constant of primary importance as far as the stopping substance is concerned is its mean excitation potential. The mean excitation potential is defined as the product of all excitation levels in the substance, $\hbar\omega_{ik}$, each weighted exponentially by its respective oscillator strength, f_{ik}:[2]

$$I = \hbar \prod \omega_{ik}^{f_{ik}}, \qquad (2)$$

where

$$\sum_{ik} f_{ik} = 1.$$

This formula would offer a means of calculation of I, but, except for the lightest of elements, a very impractical one. I is usually taken as an experimentally adjustable constant.

Bloch has shown, using the statistical model of the atom, that in the Thomas-Fermi approximation one has

$$I = KZ, \tag{3}$$

where K is an adjustable constant.[3] Using the more accurate Thomas-Fermi-Dirac model, Jensen found[4]

$$I_0 = K_0 (1 + k_0 Z^{-2/3}) Z. \tag{4}$$

The index 0 refers to isolated atoms. This function is plotted in Fig. 1 as the solid line.

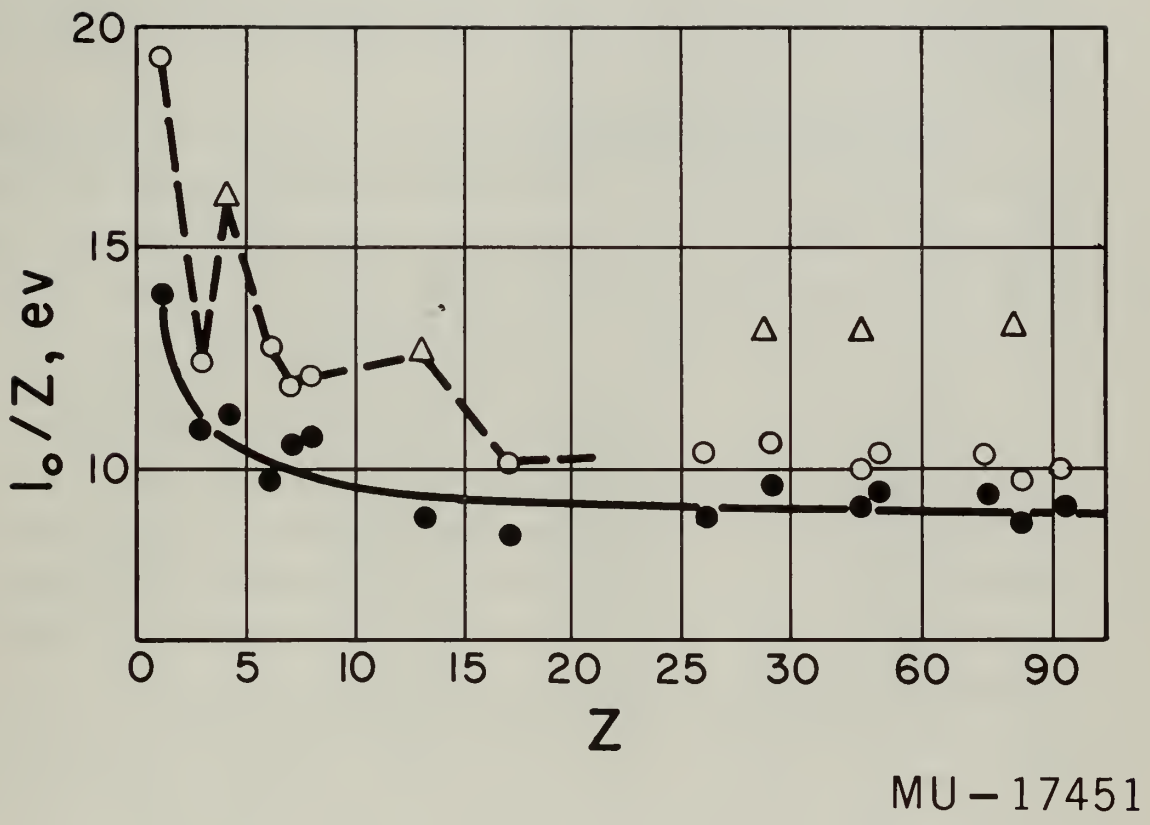

Fig. 1. Experimental mean excitation potentials and the statistical atomic model. O: I/Z of bound atoms measured with 340-Mev protons and evaluated relative to I_{Al} = 165 ev; ●: I_0/Z of isolated atoms. Δ: I/Z measured with 10-20-Mev protons and corrected for inner shells. The corrections apparently underestimate the stopping -power deficiencies of inner shells at low energies.

II. EXPERIMENTAL

Since at high energies the corrections applied to the Bethe formula for valence-shell effects are negligible, the 742-Mev protons from the Berkeley cyclotron seem to be a natural choice for the incident particles. In addition, this energy range would serve as a check on the 340-Mev Bakker and Segrè data.[5]

Figure 2 is a reproduction of a slide used by Werner Brandt at the Gatlinburg Meeting on Penetration (September, 1958), and compares the effective mean excitation potentials (without corrections), measured by Burkig and MacKenzie at UCLA in 1957,[6] with the fluctuations of the electron densities in the periodic system. One can notice slight but significant trends in the I values, which are parallel to the electron density wherever the accuracy in I is high enough. The second maximum should have been shown clearly by Mo(42) and Rh(45), but unfortunately these were the poorest foils and hence gave the least accurate data in the series. Lead showed an "anomalously" high value and needs an independent check. Thorium, on the other hand, confirmed the expected trend.

On the basis of this diagram and on the advice of Dr. Brandt the following metals were chosen as target elements: Be(4), Al(13), Fe(26), Cu(29), Ag(47), W(74), Au(79), Pb(82), and U(92). It was decided to use enough absorber to degrade the protons approximately 15% in momentum or from 742 Mev to 570 Mev in kinetic energy. In each case an equivalent amount of absorber was to be used so that the results could be compared on a relative basis with aluminum as the standard. (See Table I) Adequate information exists on Cu, Al, Ag, Pb, and Be to determine the amount of absorber required. Specifically, the tables and graphs in UCRL-2426 (rev.)[7] were used. To determine the equivalent thickness of Fe, W, Au, and U a numerical integration of Bethe's formula was performed using values of I previously determined by Bakker and Segrè (see Appendix A). Clearly these values are not precise. To provide for a means of interpolation in order to use the precise equivalent amounts of absorbers for the relative comparison, an additional length of aluminum absorber is to be added

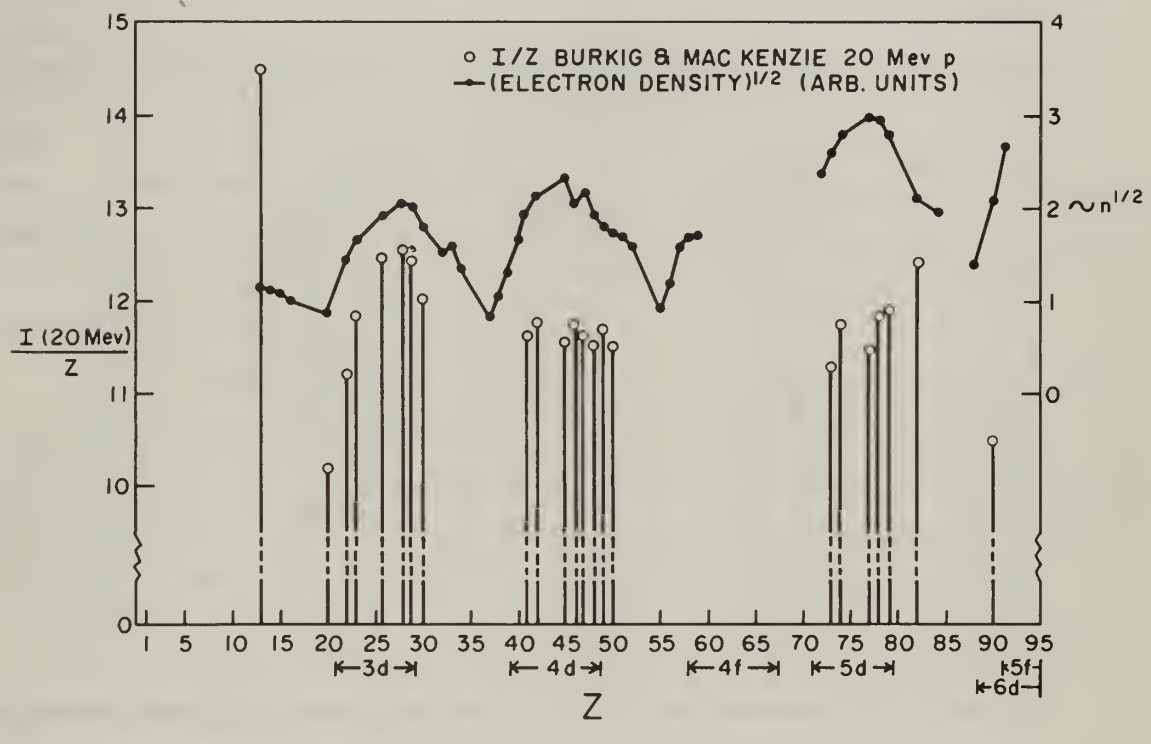

Fig. 2. Mean excitation potential compared with electron density. (From Werner Brandt, Gatlinburg Meeting on Penetration, Sept. 1958.)

to each absorber in order to provide an additional point. This absorber "shim," 9 g/cm^2 of aluminum, is to be placed first on the "upstream" and then "downstream" side of the various absorbers and the results averaged to give the effect of adding this additional absorber in the middle. The equivalent values of the aluminum shim are listed in Table II.

Table I

Equivalent absorber thicknesses

Absorber	Density	Length		
	(g/cm^3)	(g/cm^2)	(cm)	(in.)
Be(4)	1.85	85	45.94	18.09
Al(13)	2.70	89	32.98	12.98
Fe(26	7.85	91	11.59	4.56
Cu(29)	8.93	101	11.30	4.45
Ag(47)	10.49	110	10.49	4.13
W(74)	18.60	115	6.20	2.44
Au(79)	18.88	118	6.24	2.46
Pb(82)	11.34	133	11.73	4.62
U(92)	18.70	125	6.68	2.63

Table II

Equivalent value of Al shim

Absorber	Equiv. value[a]	Thickness (g/cm^2)
Be(14)	1.024	9.216
Al(13)	1.000	9.000
Fe(26)	0.906	8.154
Cu(29)	0.875	7.875
Ag(47)	0.789	7.101
W(74)	0.680	6.120
Au(79)	0.676	6.084
Pb(82)	0.660	5.940
U(92)	0.630	5.670

[a] mass stopping power

The experimental setup is shown in Fig. 3. The full energy of the 184-inch cyclotron is used, 742 Mev. The proton beam passes through a pair of jaws reducing it to 1/16 in. in the horizontal dimension. The beam then passes through focusing and bending magnets and comes to a focal point 1 foot within the physics cave. This point is the physical center of the absorbers. The beam will then pass through a focusing magnet (three-element quadrupole), and a bending magnet in which the beam will be momentum-analyzed, and then fall upon x-ray film placed at the focal point of the quadrupole.

The procedure will be to obtain an x-ray photograph of the full beam and then a photo of the beam with the absorber in place for each of the elements listed. In addition, photos will be taken with the aluminum shim as previously explained.

The density of the developed x-ray film will be proportional to the number of protons striking it. By reading the film with a densitometer one can obtain a plot of the numbers of protons versus their positions on the film. In order to facilitate density measurements a duplicate of each of the exposures mentioned above will be made at precisely one-half the time for the original. Then, for example, the maximum intensity on the second exposure will be exactly one-half that of the maximum intensity on the first, and can be used as the reference for finding the points of half-maximum intensity on the first film. This procedure can then be extended ad infinitum throughout the intensity spectrum. The plot of numbers of protons versus film positions is expected to look like Fig. 4. In addition, by the use of wire orbits, a plot of energy versus position on film can be made. This plot should look something like Fig. 5. The two graphs can then be combined to form a plot of number of protons versus energy. An example of this type of plot is shown in Fig. 6. In general it has the same shape as Fig. 4. This plot (Fig. 6) will be the tool for describing the experimental results.

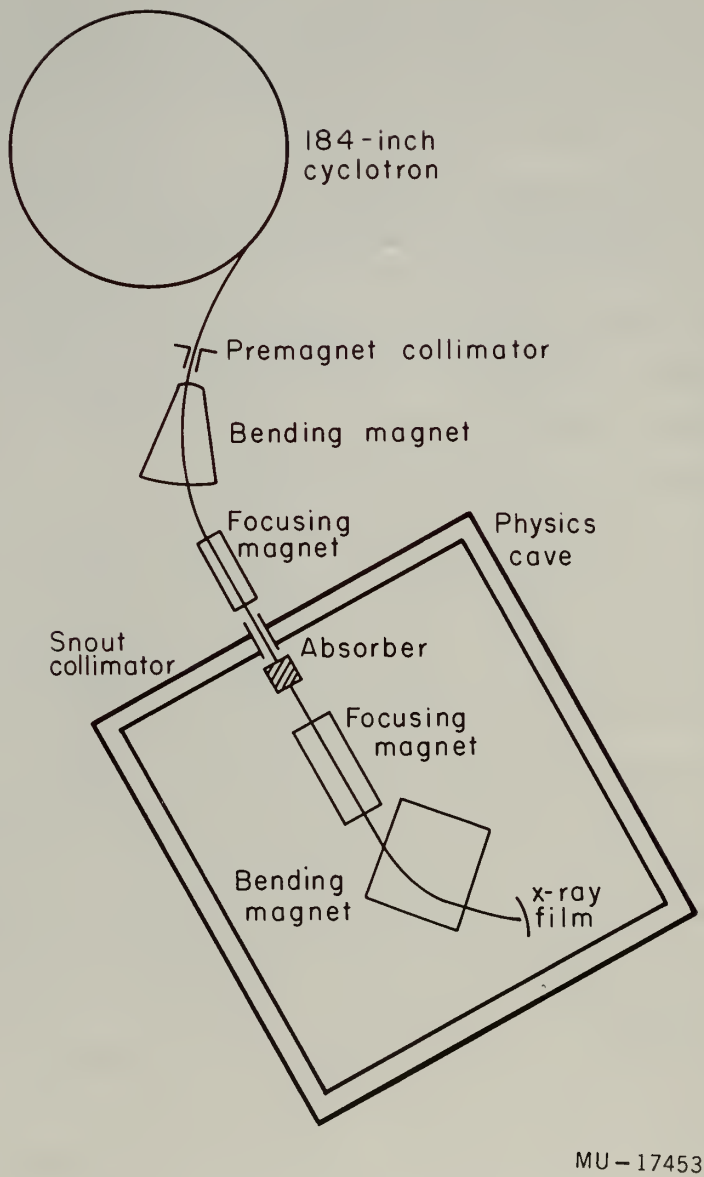

Fig. 3. Experimental setup, showing placement of magnets. Not to scale.

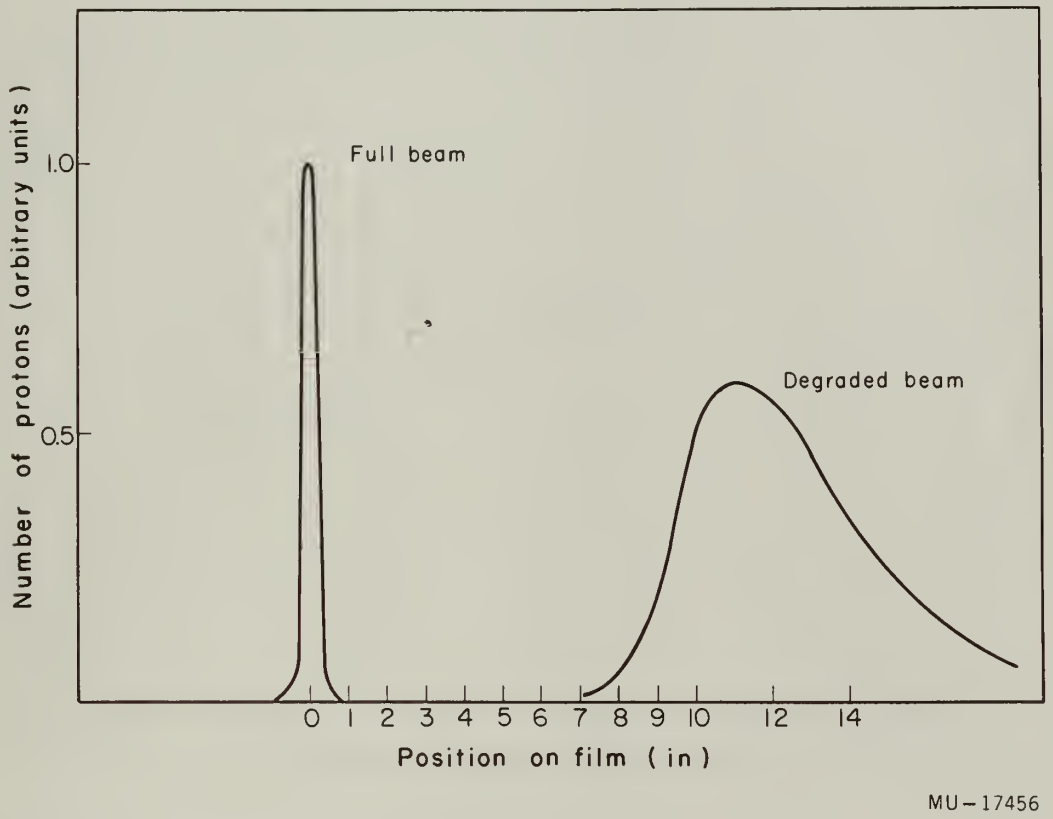

Fig. 4. Expected general contour of plot of the number of protons, i.e., the film density, versus position on an x-ray film after undergoing magnetic analysis. Two curves are shown: that of the full-energy proton beam of the 184-inch cyclotron, 742 Mev; and that of the same beam after approximately 15% momentum degradation.

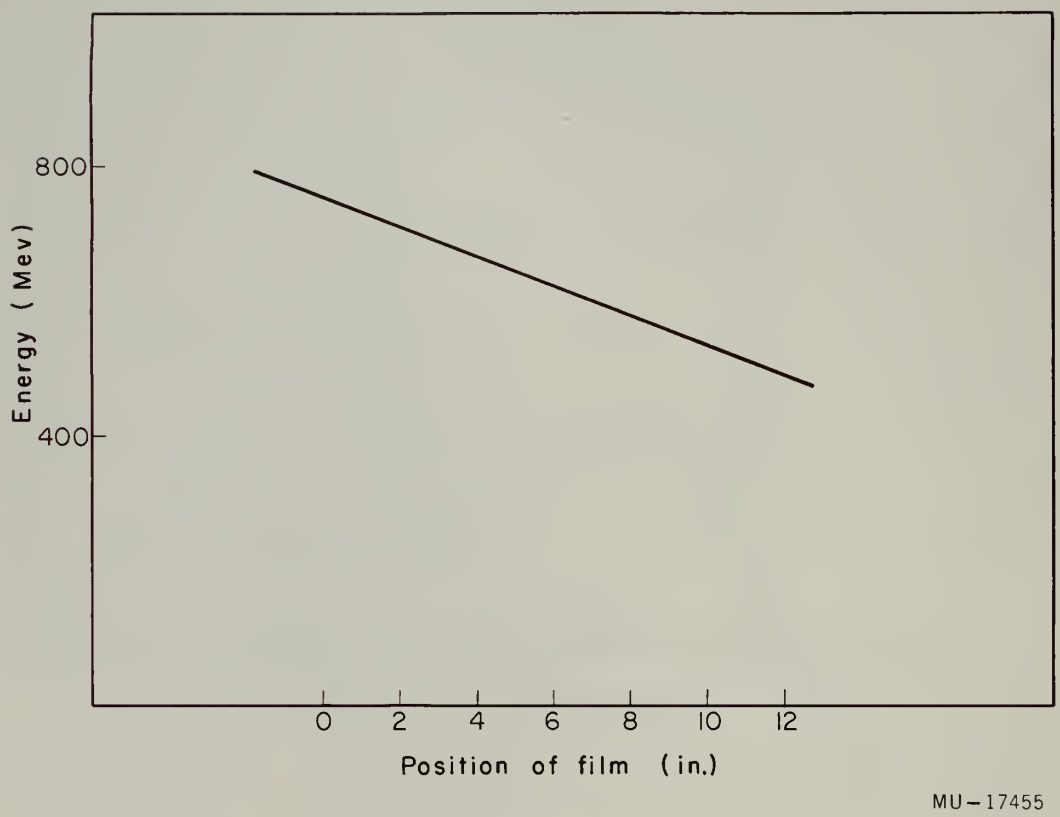

Fig. 5. Expected general contour of the results of a wire-orbit analysis of an analyzing magnet.

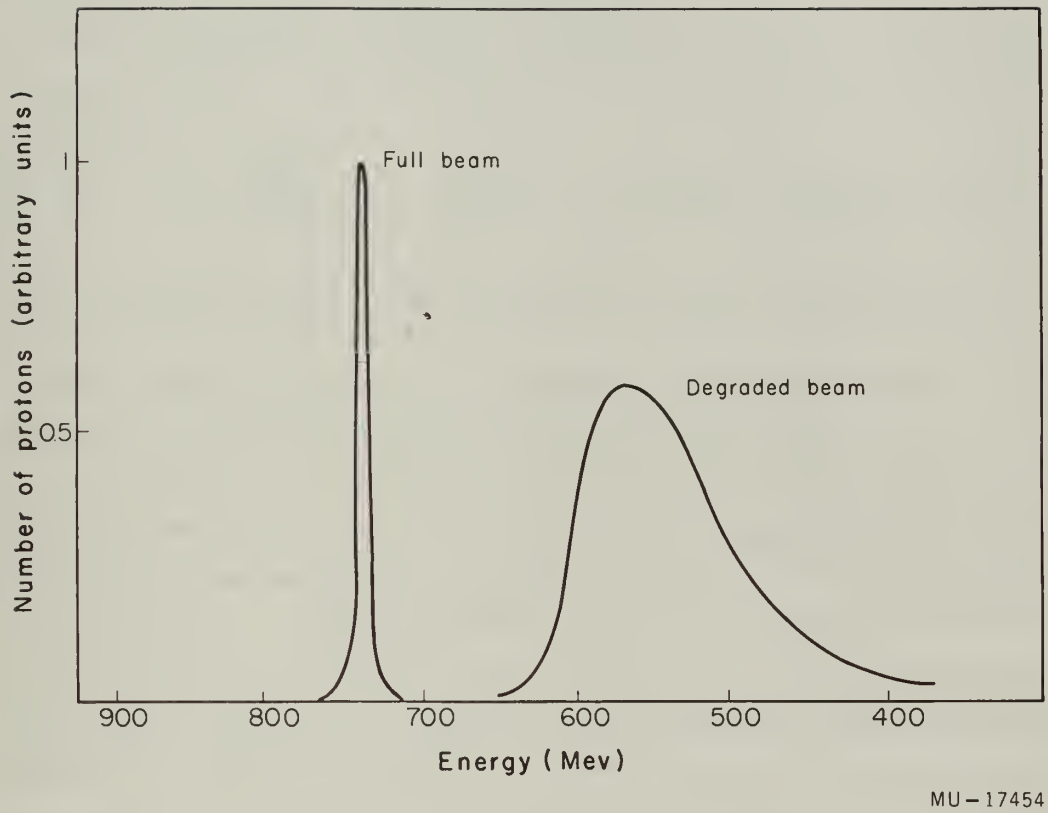

Fig. 6. Expected results of the combination of data obtained from figures 4 and 5 showing the energy spectrum of the full-energy proton beam, 742 Mev, and the same beam after approximately 15% momentum degradation.

III. DATA ANALYSIS

For determination of the mean energy loss through each absorber the center of gravity of the two curves of Fig. 6 must be found. This can be done easily for the first curve, representing the full beam of protons undegraded. However, because of close collisions of protons and electrons the second curve has, theoretically, an infinite tail. Obtaining this infinite tail is not practicable experimentally, so that it must be supplied by a theoretical calculation. The observed ranges of individual particles from any monoenergetic source will show a substantially normal distribution about the mean range. Because the very hard collisions are few in number, the actual distribution is somewhat asymmetric, with a long tail in the direction of the short ranges, and a mean range which is slightly shorter than the modal range.[8] For the approximation of this tail, the collisions suffered by the protons with the electrons of the absorbers will be divided into two classes, "near" and "far." The so-called near collisions are those responsible for the occasional large energy losses and the far collisions are those contributing only to the mean energy loss, but introducing negligible energy-loss fluctuation. In other words, each proton will suffer approximately the same minimum energy loss and may in addition suffer a near collision (or collisions) resulting in a much greater energy loss. Each absorber will then be divided into a number of equal segments in which the probability of a near collision is known, the energy loss will be computed for this one segment, and the resulting spectrum will be "folded" into itself as many times as there are segments. It is hoped that this spectrum will fit the experimental curve and provide the needed tail. This procedure seems valid in that the so-called near collisions are those in which the binding energies of the electrons are insignificant, and this is the assumption made originally by neglecting the corrections to Bethe's formula.

By this means of completing the graph for the degraded protons, the center of gravity of the curve can be found and the mean energy loss determined. This procedure would be done for each of the elements. By interpolation between the two curves, obtained by use of the

aluminum shim, for each of the elements the thickness of absorber equivalent to aluminum will be determined. The relative mass stopping power of each element will be calculated by dividing the amount of aluminum (in g/cm^2) by the amount of the element (in g/cm^2) needed to produce the same mean energy loss.

In addition, the stopping power per electron is, from Bethe's formula,

$$\frac{-\frac{dE}{dX}}{NZ} = \frac{4\pi e^4 z^2}{mv^2}\left[\ell n \frac{2mv^2}{I} - \ell n(1-\beta^2)-\beta^2\right].$$

The relative stopping power per electron with respect to aluminum is

$$q = \frac{-\ell n I + [\ell n\, 2mv^2 - \ell n(1-\beta^2)-\beta^2]}{-\ell n I_{A\ell} + [\ell n\, 2mv^2 - \ell n(1-\beta^2)-\beta^2]} .$$

This quantity can be easily calculated by multiplying the relative mass stopping power by

$$\frac{A}{A_{A\ell}} \times \frac{Z_{A\ell}}{Z} .$$

Thus the means for calculating I is apparent. In this calculation the value of I = 150 ev for aluminum is used.[9]

From the values of I calculated, a curve of I/Z versus Z will be plotted. This curve will in general look like Fig. 1. The value of the Bloch "constant" can then be compared with previously obtained values.

In order to determine the length of absorber traversed by the protons a correction for multiple scattering must be made. In the usual approximate correction, the observed range is expressed as a projection of the mean range:[10]

$$R_{obs} = \sum_i \ell_i \cos\theta_i \simeq \sum_i \ell_i (1 - \tfrac{1}{2}\theta_i^2)$$

$$= R_{mean} - \frac{1}{2} \sum_i \ell_i \theta_i^2 ,$$

where ℓ_i is the distance between the ith and the (i-1)st small-angle collision and θ_i is the direction with respect to the beam axis after the ith collision. Therefore we have

$$R_{mean} - R_{obs} = \Delta R = \frac{1}{2} \int_0^{R_{obs}} \left\langle \theta_S^2(x) \right\rangle \, dx$$

where $\left\langle \theta_S^2(x) \right\rangle$ is the mean square deviation in angle from the normal direction and x is the projected distance in the absorber. Also,

$$\theta_{rms} = \sqrt{\left\langle \theta_S^2(x) \right\rangle} = \frac{21 \text{ Mev}}{\beta c p} \sqrt{t},$$

where t is the absorber thickness measured in radiation lengths.[11] Using the value[12]

$$\left\langle \theta^2(x) \right\rangle = \int_x^{R_0} 8\pi N e^4 Z^2 G (pv)^{-2} \, dx,$$

Bichel, Mozley, and Aron found[13]

$$\frac{\Delta R}{R} = (R_{mean} - R_{obs})/R_{mean}$$

$$= \frac{G m_0 c^2 Z}{(M_0 c^2)^2} \frac{\left(\int_0^{E_0} \frac{\beta^2}{B/Z} \, dE \int_E^{E_0} \frac{-1\beta^2}{\beta^2 (B/Z)} \, dE \right)}{\int_0^E \frac{\beta^2}{B/Z} \, dE},$$

Where $G = 2\ell n\, 181\, Z^{-1/3}$, B is the stopping number of the atom,

$$B = Z \left[\ell n \frac{2mv^2}{I(1-\beta^2)} - \beta^2 \right],$$

and m_0 is the rest mass of the electron. The ratio $\Delta R/R$ is a slowly varying function of the energy, amounting to several percent for high Z.

The corrections found by these experimenters appear in Table III. In each case it is clear that as Z increases the correction for multiple scattering increases, and as E increases this correction decreases.

Table III

Multiple-scattering corrections

Element	E (Mev)	$\frac{\text{Range}_{obs}}{\text{Path length}}$ [a]
Be	17.340	0.9990
	9.588	0.9988
Al	17.836	0.9962
	14.971	0.9960
	11.820	0.9956
	6.150	0.9943
Cu	17.893	0.9900
	9.938	0.9872
Ag	17.923	0.9818
	10.022	0.9759
Au	17.549	0.9626
	9.698	0.9475

[a] correction for multiple scattering

IV. ACKNOWLEDGMENT

The aid and counsel extented by Professors Emilio Segrè and Owen Chamberlain, and the help of Dr. Lewis E. Agnew, Jr. with the magnetic development are gratefully acknowledged.

This work was done under the auspices of the U. S. Atomic Energy Commission.

APPENDIX

A. Determination of Absorber Thicknesses

1. Fe, W, Au, and U

Since no usuable data exist on these elements, a numerical integration of Bethe's equation was performed in order to determine the absorber thickness. The total desired energy drop was divided into twelve equal steps such that the change in β was constant, 0.004. The energy increment was then calculated from

$$E = m_0 \gamma c^2,$$

where

$$\gamma = \frac{1}{\sqrt{1-\beta^2}} .$$

Therefore we have

$$\Delta E = m_0 c^2 \beta \gamma^2 \Delta\beta = 3.752\, \beta \gamma^3 \text{ (Mev)}.$$

The integration on Bethe's equation was performed by determining

$$\Delta\left(\frac{dE}{dx}\right) = \frac{2B\rho Z}{\beta A}\left[-\frac{\ell n\, G\beta^2\gamma^2}{\beta^2} + \frac{\gamma^2}{G}\right]\Delta\beta,$$

where

$$B = \frac{4\pi e^4 Z^2 N_0}{m_0 c^2} = 7.21\times10^{-7}\ \frac{\text{g cm}^4}{\text{sec}^2}\ \frac{\text{atoms}}{\text{g-atom}} .$$

$$G = \frac{1.022}{I}\times 10^6.$$

The values determined appear in Tables IV and V. Graphs of the resultant variation in dE/dx are shown in Figs. 7 through 10.

2. Be, Al, Cu, Ag, and Pb

Sufficient data on these elements exist in UCRL-2426 (rev).[6]

3. Summary

The absorber thicknesses to be used were given in Table I.

Table IV

Calculated results of numerical integration of Bethe's equation, showing incremental values of dE/dx.

β	ΔE (Mev)	E (Mev)	$\Delta \frac{dE}{dx}$ (Mev/cm)				$\frac{dE}{dx}$			
			Fe	W	Au	U	Fe	W	Au	U
0.825	17.2	742	0.214	0.502	0.484	0.461	13.62	24.95	24.99	23.24
0.821	16.5	724.8	0.217	0.506	0.488	0.480	13.83	25.45	25.47	23.70
0.817	15.9	708.3	0.220	0.510	0.492	0.484	14.05	25.96	25.96	24.18
0.813	15.4	692.4	0.221	0.513	0.495	0.487	14.27	26.47	26.45	24.66
0.809	14.9	677.0	0.224	0.517	0.499	0.490	14.49	26.98	26.95	25.14
0.805	14.4	662.1	0.227	0.536	0.502	0.494	14.71	27.50	27.45	25.63
0.801	14.0	647.7	0.230	0.536	0.521	0.497	14.94	28.04	27.95	26.12
0.797	13.6	633.7	0.233	0.545	0.525	0.501	15.17	28.58	28.47	26.62
0.793	13.2	620.1	0.236	0.551	0.532	0.523	15.40	29.12	28.99	27.12
0.789	12.7	606.9	0.237	0.552	0.533	0.524	15.64	29.67	29.52	27.64
0.785	12.3	594.2	0.240	0.556	0.537	0.528	15.92	30.22	30.05	28.16
0.781	12.0	581.9	0.244	0.577	0.557	0.532	16.16	30.78	30.59	28.69
0.777	11.7	569.9	0.247	0.581	0.561	0.536	16.40	31.36	31.15	29.23

Table V

Calculated results of numerical integration of Bethe's equation, showing absorber thicknesses required to obtain desired energy degradation

Energy range (Mev)	ΔE (Mev)	$\overline{\frac{\Delta E}{\Delta x}}$ (Mev/cm)				Δx_i (cm)			
		Fe	W	Au	U	Fe	W	Au	U
742.0 - 724.8	17.2	13.72	25.20	25.23	23.47	1.25	0.68	0.68	0.73
724.8 - 708.3	16.5	13.94	25.70	25.72	23.94	1.18	0.64	0.64	0.69
708.3 - 692.4	15.9	14.16	26.22	26.20	24.42	1.12	0.61	0.61	0.65
692.4 - 677.0	15.4	14.38	26.73	26.70	24.90	1.07	0.58	0.58	0.62
677.0 - 621.1	14.9	14.60	27.24	27.20	24.38	1.02	0.55	0.56	0.61
621.1 - 647.7	14.4	14.82	27.77	27.70	25.88	0.97	0.52	0.52	0.56
647.7 - 633.7	14.0	15.05	28.31	28.21	26.37	0.93	0.49	0.50	0.53
633.7 - 620.1	13.6	15.28	28.85	28.73	26.87	0.89	0.47	0.47	0.51
620.1 - 606.9	13.2	15.52	29.40	29.26	27.38	0.85	0.45	0.45	0.48
606.9 - 594.2	12.7	15.78	29.95	29.79	27.90	0.80	0.42	0.43	0.46
594.2 - 581.9	12.3	16.04	30.50	30.32	28.42	0.77	0.40	0.41	0.43
581.9 - 569.9	12.0	16.28	31.08	30.87	28.96	0.74	0.39	0.39	0.41
					$\sum_i x_i$ =	11.59	6.20	6.24	6.68

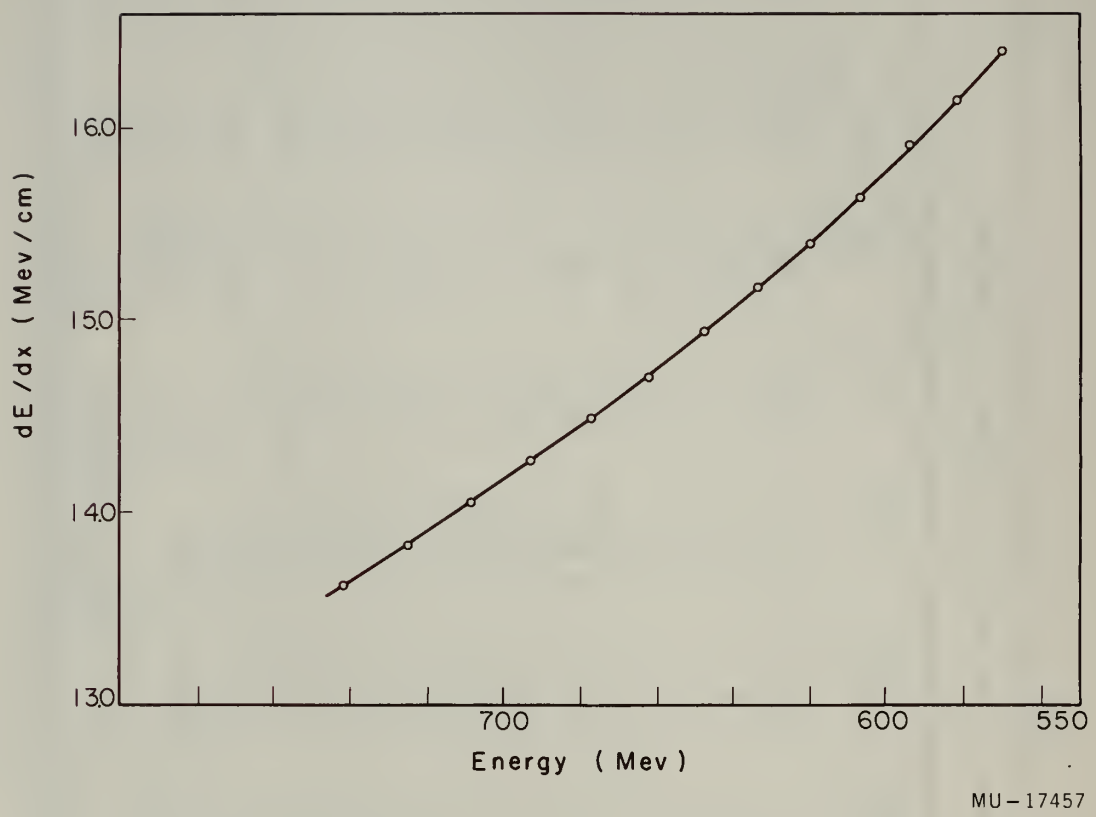

Fig. 7. Calculated range-energy curve for Fe.

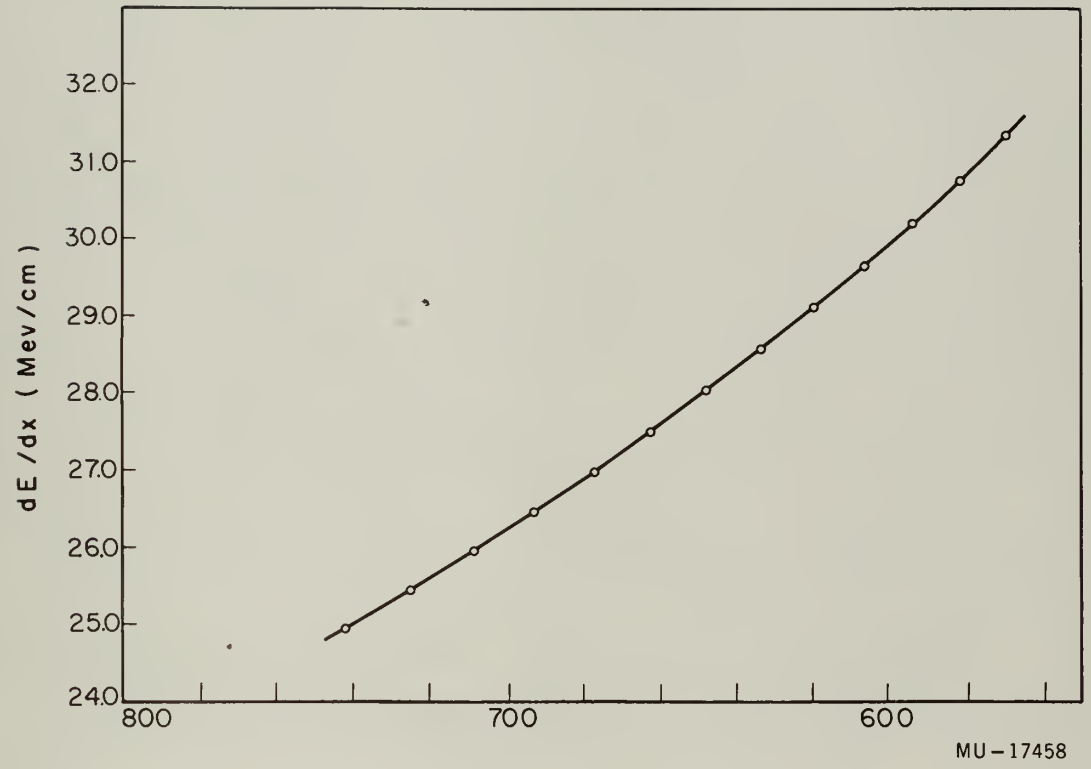

Fig. 8. Calculated range-energy curve for W.

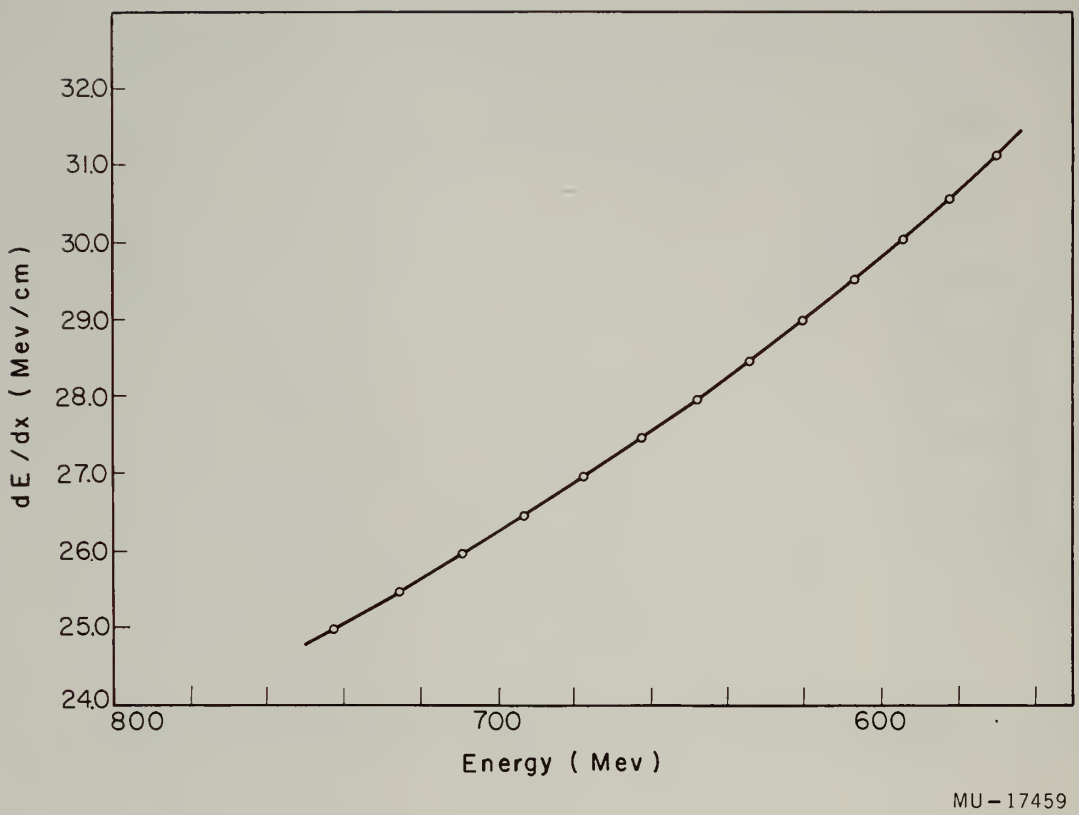

Fig. 9. Calculated range-energy curve for Au.

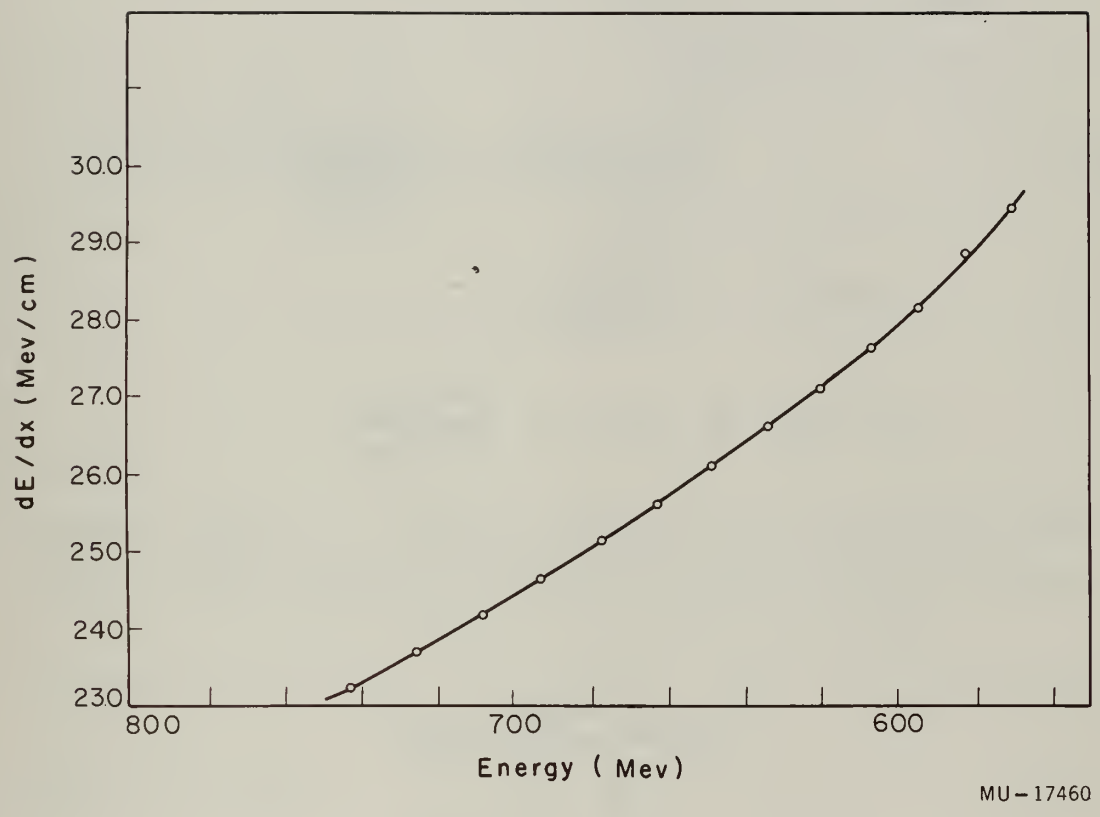

Fig. 10. Calculated range-energy curve for U.

B. Bending-Magnet Analysis

1. Angle of Bending

If the $H\ell$ of the magnet and the $H\rho$ of the particle are known, the following is the derivation for the angle of bending (See Fig. 11):

$$\sin \frac{\theta}{2} = \frac{\ell}{2\rho} \quad ,$$

$$\rho = \frac{(H\rho)_{\text{particle}}}{H_{\text{magnet}}} = \frac{(H\rho)_{\text{part.}}}{(H\ell)_{\text{mag.}}} \times \ell;$$

$$\therefore \sin \frac{\theta}{2} = \frac{(H\ell)_{\text{mag.}}}{2(H\rho)_{\text{part.}}} \quad ;$$

$$\text{if } \sin \frac{\theta}{2} \simeq \frac{\theta}{2}, \text{ then } \theta \simeq \frac{(H\ell)_{\text{mag.}}}{(H\rho)_{\text{part.}}} \quad .$$

This approximate formula works well for θ less than 1 radian.

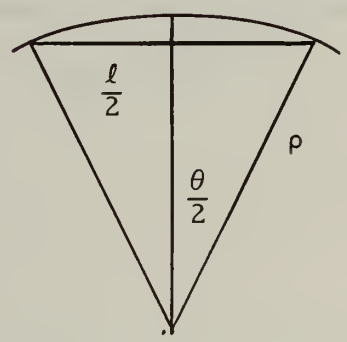

Fig. 11. Path of a particle in a magnetic field.

2. Vertical Focusing in an Analyzing Magnet

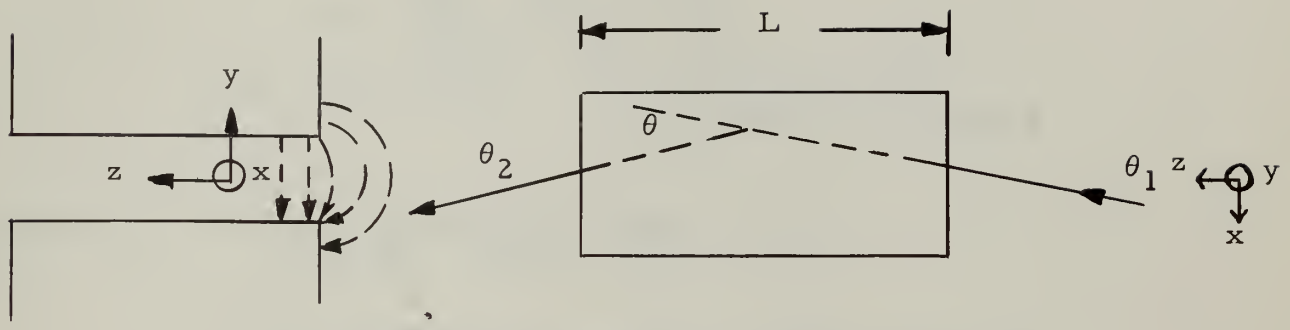

Fig. 12. Side and top views of typical bending magnet, showing field configurations and entrance and exit angles.

In Fig. 12, let $\theta_1 = \theta_2 = \frac{\theta}{2}$ and $\tan\theta_1 = -\frac{v_x}{v_y}$. From Maxwell's equations we have

$$\nabla \times \vec{H} = 0,$$

$$\frac{\partial H_y}{\partial x} - \frac{\partial H_x}{\partial y} = 0,$$

$$\frac{\partial H_z}{\partial y} - \frac{\partial H_y}{\partial z} = 0,$$

$$\frac{\partial H_x}{\partial z} - \frac{\partial H_z}{\partial x} = 0; \qquad (1)$$

$$\nabla \cdot \vec{H} = 0,$$

$$\frac{\partial H_x}{\partial x} + \frac{\partial H_y}{\partial y} + \frac{\partial H_z}{\partial z} = 0.$$

I shall let $H_x = 0$; then

$$\frac{\partial H_x}{\partial y} = \frac{\partial H_x}{\partial z} = \frac{\partial H_x}{\partial x} = 0, \qquad (2)$$

and substituting Eqs. (2) into (1), one has

$$\frac{\partial H_y}{\partial x} = \frac{\partial H_z}{\partial x} = 0, \quad \frac{\partial H_z}{\partial y} = \frac{\partial H_y}{\partial z}, \quad \frac{\partial H_y}{\partial y} = -\frac{\partial H_z}{\partial z}.$$

Using Gaussian units,

$$F_y = (e/c\ \vec{v} \times \vec{H})_y$$

$$= e/c(v_z H_x - v_x H_z) = -e/c\ v_x H_z.$$

Assuming $\frac{\partial H_z}{\partial y}$ is constant leads to

$$H_z = \int_0^y \frac{\partial H_z}{\partial y}\,\Delta y = \frac{\partial H_z}{\partial y}\ y = \frac{\partial H_y}{\partial z}\ y.$$

Therefore

$$F_y = -e/c\ v_x H_z = -e/c\ v_x \frac{\partial H_y}{\partial z}\ y.$$

The momentum imparted to the particle in the y direction is

$$\Delta p_y = \int F\, dt = \int F_y \frac{dz}{v_z} = -\frac{e}{c}\int \frac{v_x}{v_z}\, y\, \frac{dH_y}{dz}\, dz$$

$$= \frac{e}{c} \tan\theta_1\, y \left(\frac{\partial H_y}{dz}\, dz\right) = \frac{e}{c} \tan\theta_1\, y\, \Delta H_y \ .$$

Defining $\delta = \Delta p_y/p$, where $p = eH\rho/c$, one has

$$\delta = \frac{(e/c)\tan\theta_1\, y\, \Delta H_y}{(e/c)H\rho} = \tan\theta_1\, \frac{y}{\rho}\, \frac{\Delta H_y}{H} \ .$$

In the pole gap $H = H_y$, and ΔH_y is the increase of H_y from a place of zero field to the edge of the pole tips, where H_y becomes uniform and equal to H. Therefore

$$\Delta H_y = H$$

and

$$\delta = \tan\theta_1\, \frac{y}{\rho} \ . \qquad (3)$$

I have assumed H_y small until reaching the pole tips, so that v_x is constant. From Fig. 13 we have

$$y = S_0\beta = S_i\alpha.$$

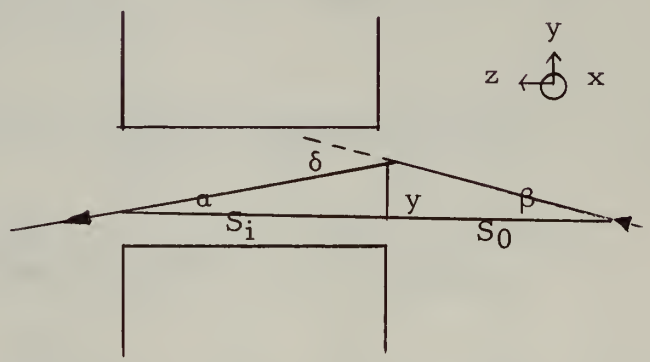

Fig. 13. Vertical bending at pole tips due to field variations.

Therefore

$$\delta = \alpha + \beta = \frac{y}{S_i} + \frac{y}{S_0}$$

or

$$\frac{1}{S_0} + \frac{1}{S_i} = \frac{\delta}{y} = \frac{1}{f} \ ;$$

from Eq. (3),

$$\frac{1}{f} = \frac{\delta}{y} = \frac{\tan\theta_1}{\rho} \ .$$

This means that f is independent of the height at which the particle hits the entrance of the magnet. This independence contributes the focusing action in the vertical plane. The principal planes are assumed to be the ends of the magnet. In terms of the total angle of bending,

$$\frac{1}{f} = \frac{\tan\theta/2}{\rho} \ . \qquad (4)$$

3. Change in Vertical Focal Length with a Change in Momentum

Given $f = \frac{\rho}{\tan \theta_1}$, $\sin \theta_1 = \frac{L}{2\rho}$,

we have

$$\tan \theta_1 = \frac{\sin \theta_1}{\sqrt{1 - \sin^2 \theta_1}} = \frac{1}{\sqrt{\frac{1}{\sin^2 \theta_1} - 1}} .$$

Therefore

$$f = \rho \sqrt{\frac{1}{\sin^2 \theta_1} - 1} = \rho \sqrt{\frac{4\rho^2}{L^2} - 1} ,$$

since

$$\rho = \frac{pc}{eH} , \qquad f = \sqrt{\frac{4\rho^4}{L^2} - \rho^2} ,$$

and

$$\Delta f = \frac{\rho}{f} \left(\frac{8\rho^2}{L^2} - 1 \right) \Delta \rho,$$

or, using

$$\Delta \rho = (c/e\ B)\, \Delta p = \rho\, \Delta p/p,$$

$$\Delta f = \frac{c^2 p}{e^2 H^2 f} \left(\frac{8 c^2 p^2}{e^2 H^2 L^2} - 1 \right) \Delta p,$$

$$\Delta f = \frac{\rho^2}{f} \left(\frac{8p^2}{L^2} - 1 \right) \frac{\Delta p}{p} . \qquad (5)$$

4. Dispersion in an Analyzing Magnet

In order to determine the dispersion particles of various momenta passing through an analyzing magnet, it is necessary to find distance d in Fig. 14. Figure 14 shows two particle tracks, with point (h, k) being the center of curvature of the lesser momenta particle. From the geometry we have

$$h = -L/2 + \rho' \sin(\theta/2),$$

$$k = \rho' \cos(\theta/2).$$

The equations for the circles s and s' are

$$(x - 0)^2 + (y - \rho\cos(\theta/2))^2 = \rho^2,$$

$$(x + \frac{L}{2} - \rho' \sin(\theta/2))^2 + (y - \rho' \cos(\theta/2))^2 = \rho'^2.$$

To find d it is then necessary to find the intersection of the circle s' and the line x = L/2. Note that we have

$$\sin(\theta/2) = \frac{L/2}{\rho}, \qquad \cos(\theta/2) = \frac{\sqrt{\rho^2 - L^2/4}}{\rho}.$$

Therefore the equation for the circle s' is

$$[x + (\rho - \rho')\sin(\theta/2)]^2 + (y - \rho' \cos(\theta/2))^2 = \rho'^2$$

$$= x^2 + 2x(\rho-\rho')\sin(\theta/2) + (\rho-\rho')^2 \sin^2(\theta/2) + y^2 - 2y\rho' \cos(\theta/2) + (\rho')^2\cos^2(\theta/2) = \rho'^2$$

$$= x^2 + 2x(\rho-\rho')\sin(\theta/2) + \rho^2\sin^2(\theta/2) - 2\rho\rho' \sin^2(\theta/2) + y^2 - 2y\rho' \cos(\theta/2) = 0.$$

Now at x = L/2 (i.e., the intersection of circle s' and line x = L/2), we have

$$\frac{L^2}{4} + L(\rho-\rho')\sin(\theta/2) + \rho^2 \sin^2(\theta/2) - 2\rho\rho' \sin^2(\theta/2) + y^2 - 2y\rho' \cos(\theta/2) = 0.$$

This reduces to

$$y = \rho' \cos(\theta/2) - \sqrt{\rho'^2 \cos^2(\theta/2) - L^2(1 - \rho'/\rho)}.$$

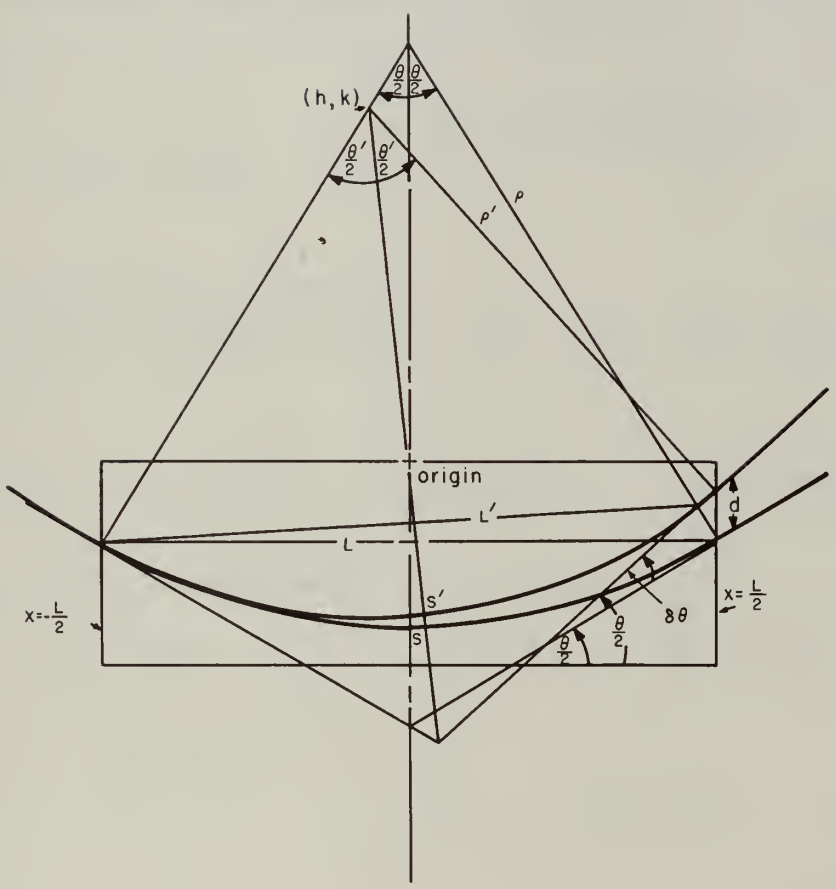

Fig. 14. Dispersion in an analyzing magnet of charged particles of different momenta.

Observing

$$\sin\frac{\theta}{2} = \frac{L}{2\rho} \quad , \quad \sin\frac{\theta'}{2} = \frac{L'}{2\rho'} \quad , \quad \frac{\theta'}{2} = \frac{\theta}{2} + \frac{\delta\theta}{2} \quad ,$$

we see

$$\sin\frac{\theta'}{2} = \sin\left(\frac{\theta}{2} + \frac{\delta\theta}{2}\right) = \frac{L'}{2\rho'} = \sin\frac{\theta}{2}\cos\frac{\delta\theta}{2} + \cos\frac{\theta}{2}\sin\frac{\delta\theta}{2}$$

$$\simeq \sin\frac{\theta}{2} + \frac{\delta\theta}{2}\cos\frac{\theta}{2} \quad .$$

Further,

$$\frac{\delta\theta}{2}\cos\frac{\theta}{2} = \frac{L'}{2\rho'} - \frac{L}{2\rho} = \frac{\sqrt{L^2+d^2}}{2\rho'} - \frac{L}{2\rho} = \frac{L\sqrt{1+d^2/2}}{2\rho'} - \frac{L}{2\rho} .$$

Therefore

$$\frac{\rho}{L}\cos\frac{\theta}{2}\,\delta\theta = \frac{\rho}{\rho'}\sqrt{1+d^2/L^2} - 1$$

$$\simeq \frac{\rho}{\rho'}\left(1 - \frac{d^2}{2L^2}\right) - 1.$$

Since $\rho = L/2\sin\frac{\theta}{2}$,

we have

$$\frac{L}{2\sin\frac{\theta}{2}\,L}\cos\frac{\theta}{2}\,\delta\theta = \frac{\rho-\rho'}{\rho} + \frac{\rho}{\rho'}\left(\frac{d^2}{2L^2}\right)$$

and

$$\delta\theta = 2\tan\frac{\theta}{2}\left[\frac{\rho-\rho'}{\rho'} + \frac{\rho}{\rho'}\,\frac{d^2}{2L^2}\right] .$$

Since $p \propto \rho$

we have $$\frac{p'}{p} = \frac{\rho'}{\rho}$$

and $$\delta\theta = 2\tan\frac{\theta}{2}\left[\frac{p-p'}{p'} + \frac{p}{p'}\,\frac{d^2}{2L^2}\right] ,$$

where $$d = \rho' \cos\frac{\theta}{2} - \sqrt{\rho'^2\cos^2\frac{\theta}{2} - L^2(1-\rho/\rho')}$$

$$\approx \frac{L^2(1-\rho'/\rho)}{2\rho'\cos\frac{\theta}{2}} .$$

Therefore $$\delta\theta = 2\tan\frac{\theta}{2}\left(\frac{p-p'}{p'}\right)\left[1 + \frac{1}{2}\,\frac{p}{p'}\left(\frac{p-p'}{p'}\right)\tan^2\frac{\theta}{2}\right] .$$

The assumptions made were

$$\sin\frac{\theta}{2}\cos\frac{\delta\theta}{2} = \sin\frac{\theta}{2} , \qquad \sin\frac{\delta\theta}{2}\cos\frac{\theta}{2} = \frac{\delta\theta}{2}\cos\frac{\theta}{2} ,$$

$$\sqrt{1+\frac{d^2}{L^2}} = 1 + \frac{d^2}{2L^2} .$$

C. Wire Orbits

1. The Wire-Orbit Method

This is an experimental method for determining the path of a charged particle in a magnetic field. It is based on the analogy between the shape assumed by a current-carrying wire in a magnetic field and the path of a moving charged particle in the same field.

The motion of a charged particle in a magnetic field is described by the equation

$$\frac{mv^2}{R} = e\vec{v} \times \vec{B}$$

with the solution

$$BR = p/e. \qquad (1)$$

The forces on the wire in Fig. 15 consist of the tension, T, and the force due to the magnetic field,

$$F = i\, d\vec{\ell} \times \vec{B}\ .$$

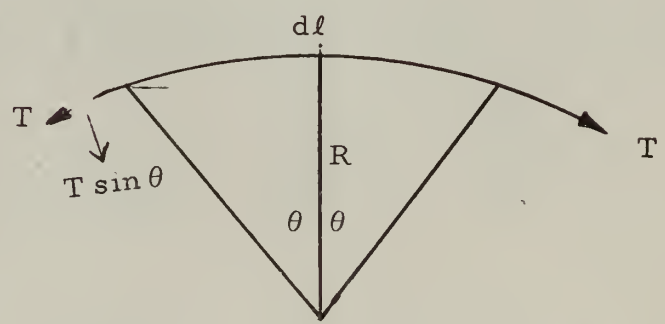

Fig. 15. Forces involved in the wire-orbit method.

Equating the forces,

$$2T \sin\theta = i\, d\ell\, B,$$

and noting

$$\sin\theta = \frac{d\ell/2}{R} \qquad \text{as } d\ell \to 0,$$

one finds

$$BR = \frac{T}{i} \quad . \qquad (2)$$

Therefore it is clear that if the ratio of tension to current in the wire is the same as the ratio of momentum to charge of the particle, the wire will assume the path of the charged particle.

The above derivation is for a constant B, but it is possible to divide the wire into many small segments where the immediate field is considered constant, and, in the limit, the wire orbit and particle path will be the same for

$$\frac{T}{i} = \frac{p}{e} \quad . \qquad (3)$$

In practice the wire should be very fine and flexible so that the force of gravity may be neglected. In workable units,

$$p(\text{Mev/c}) = \frac{2.94\ M(g)}{I(\text{amp})} \quad ,$$

where M indicates the weight attached to the wire to provide the tension.

2. Example

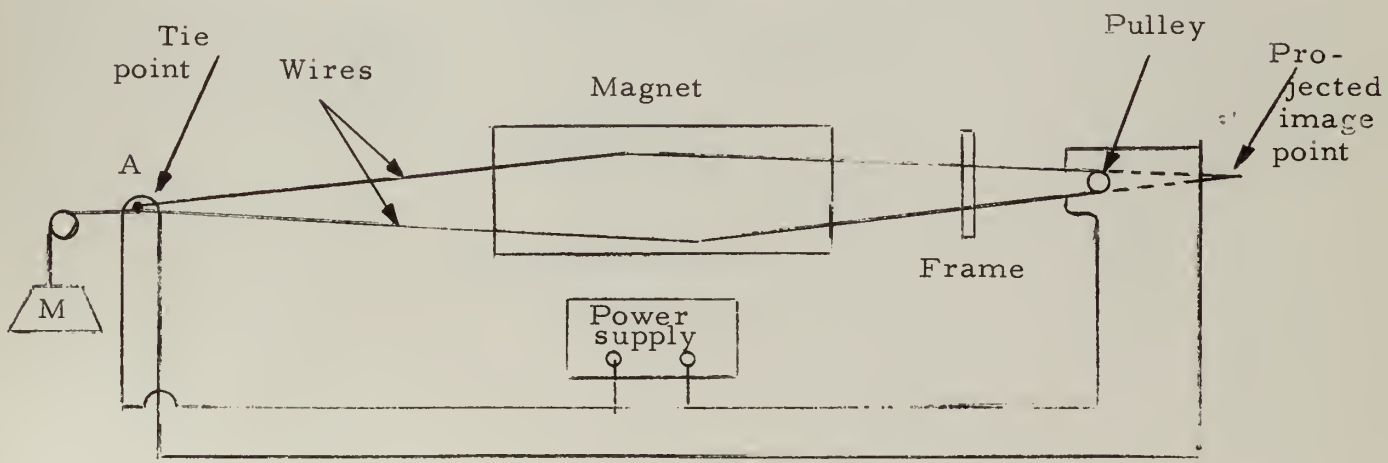

Fig. 16. Experimental setup in wire-orbit method.

A typical experimental setup for using the wire-orbit method is shown in Fig. 16. The two pieces of wire passing through the magnet are in series so that they represent two possible "rays" of particles eminating from the tie point, A. Actually the tie point must be located slightly ahead of the planned point of particle emission, since the wires occupy physical space and cannot be made to emanate from a point. The wires then pass through the magnet, past a frame for measuring their separation, and then to a point just short of a pulley. A short piece of insulated wire is tied to the current-carrying wire and then passed around the pulley. This is done so that the currents in each wire have the same direction sense. Using the tie point as the object and the intersection of the wires, as determined by a projection of the measured separation at the frame and diameter of the pulley (as in Fig. 17) as the image, one solves the focusing problem by simple geometry. In practice the current in the magnets is adjusted until the separation, s, at the frame is correct to provide the desired image point.

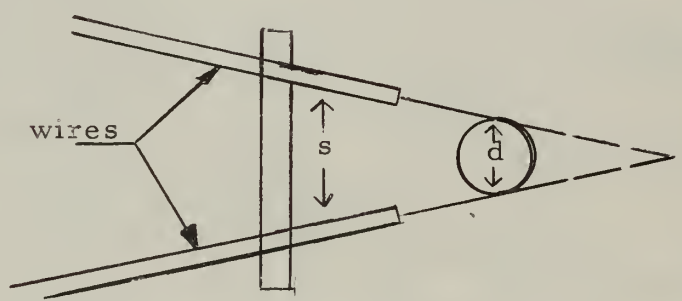

s = separation at frame

d = pulley diameter

Fig. 17. Geometric determination of focus.

REFERENCES

1. M. S. Livingston and H. A. Bethe, Revs. Modern Phys. 9, 285 (1937).
2. W. Brandt, Health Physics 1, 11-20 (1958).
3. F. Bloch, Z. Physik 81, 363-376 (1933).
4. H. Jensen, Z. Physik 106, 620-632 (1937).
5. C. J. Bakker and E. Segrè, Phys. Rev. 81, 489-492 (1951).
6. V. C. Burkig and K. R. MacKenzie, Phys. Rev. 106, 848 (1957).
7. J. H. Atkinson, Jr. and B. H. Willis, High-Energy Particle Data, Vol. II, UCRL-2426 (rev), 1957.
8. D. C. Sachs and R. J. Richardson, Phys. Rev. 83, 834 (1951).
9. R. R. Wilson, Phys. Rev. 60, 749 (1941).
10. R. Mauer and E. Segrè, Phys. Rev. 84, 191 (1951).
11. B. Rossi, High-Energy Particles, (Prentice-Hall Publishing Co., New York, 1952).
12. B. Rossi and K. Greisen, Revs. Modern Phys. 13, 240 (1941).
13. Bichel, Mozley, and Aron, Phys. Rev. 105, 1788-1795 (1957).